

Reductive Sequestration of Pertechnetate ($^{99}\text{TcO}_4^-$) by Nano Zerovalent Iron (nZVI) Transformed by Abiotic Sulfide

Dimin Fan, Roberto P. Anitori, Bradley M. Tebo, and Paul G. Tratnyek*

Division of Environmental and Biomolecular Systems, Oregon Health & Science University, 20000 NW Walker Road, Beaverton, Oregon 97006, United States

Juan S. Lezama Pacheco[†]

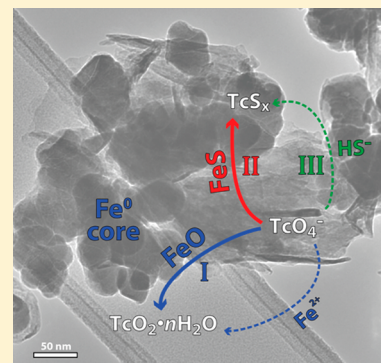
Stanford Synchrotron Radiation Lightsource, Menlo Park, California 94025, United States

Ravi K. Kukkadapu, Mark H. Engelhard, Mark E. Bowden, Libor Kovarik, and Bruce W. Arey

Environmental Molecular Sciences Laboratory, Pacific Northwest National Laboratory, Richland, Washington 99354, United States

S Supporting Information

ABSTRACT: Under anoxic conditions, soluble pertechnetate ($^{99}\text{TcO}_4^-$) can be reduced to less soluble $\text{TcO}_2 \cdot n\text{H}_2\text{O}$, but the oxide is highly susceptible to reoxidation. Here we investigate an alternative strategy for remediation of Tc-contaminated groundwater whereby sequestration as Tc sulfide is favored by sulfidic conditions stimulated by nano zerovalent iron (nZVI). nZVI was pre-exposed to increasing concentrations of sulfide in simulated Hanford groundwater for 24 h to mimic the onset of aquifer biotic sulfate reduction. Solid-phase characterizations of the sulfidated nZVI confirmed the formation of nanocrystalline FeS phases, but higher S/Fe ratios (>0.112) did not result in the formation of significantly more FeS. The kinetics of Tc sequestration by these materials showed faster Tc removal rates with increasing S/Fe between 0 and 0.056, but decreasing Tc removal rates with S/Fe > 0.224. The more favorable Tc removal kinetics at low S/Fe could be due to a higher affinity of TcO_4^- for FeS than iron oxides, and electron microscopy confirmed that the majority of the Tc was associated with FeS phases. The inhibition of Tc removal at high S/Fe appears to have been caused by excess HS^- . X-ray absorption spectroscopy revealed that as S/Fe increased, the pathway for Tc(IV) formation shifted from $\text{TcO}_2 \cdot n\text{H}_2\text{O}$ to Tc sulfide phases. The most substantial change of Tc speciation occurred at low S/Fe, coinciding with the rapid increase in Tc removal rate. This agreement further confirms the importance of FeS in Tc sequestration.



INTRODUCTION

Technetium 99 (^{99}Tc) is a weak β -emitting isotope, mainly generated from nuclear fission processes of uranium-235 and plutonium-239. Its long half-life (2.13×10^5 years) and high mobility in oxic subsurface environments (as the pertechnetate anion, $\text{Tc}^{VII}\text{O}_4^-$) make it a high priority among radionuclides that require control and remediation at U.S. Department of Energy sites.^{1–4} Under anoxic conditions and in the absence of strong complexing ligands, such as carbonate and humic substances,^{5,6} aqueous TcO_4^- is readily reduced to the much less soluble $\text{Tc}^{IV}\text{O}_2 \cdot n\text{H}_2\text{O}$. This reduction can occur by various abiotic and biotic processes (reviewed by Icenhower et al.⁷ and O'Loughlin et al.⁸). To date, most research has focused on using biogenic or abiogenic reactive Fe(II) species (aqueous, sorbed, or structural) as the reductants.^{9–12} The rationale for this focus is partly because of the natural abundance of iron oxides, and—in particular—the concurrency of Tc reduction and iron reduction observed under natural redox gradients.¹³ However, the long-term stability of Tc phases sequestered

under iron reducing conditions is uncertain due to the susceptibility of $\text{TcO}_2 \cdot n\text{H}_2\text{O}$ to reoxidation by oxygen (or nitrate) and subsequent release of TcO_4^- back into the aqueous phase.¹⁴ Although several studies have reported that the association of Tc with iron oxide minerals by chemical adsorption¹² or structural incorporation¹⁵ can significantly lower the rate of Tc^{IV} oxidation, the adequacy of these mechanisms for long-term stabilization of Tc in natural sediments is unproven, especially where it is likely to be limited due to heterogeneity of the sediments and other factors.

An alternative strategy to mitigate Tc reoxidation is to sequester Tc in a sulfide-rich environment that will favor the formation of Tc sulfide phases. Laboratory studies have demonstrated that Tc can be immobilized by Na_2S under

Received: November 26, 2012

Revised: April 17, 2013

Accepted: April 24, 2013

Published: April 24, 2013

simulated field conditions of nuclear waste tank repositories (high pH and ionic strength).^{16–18} The resulting solid was characterized as Tc_2S_7 , which was proposed to have a Tc^{IV} oxidation state, even though the stoichiometry appears to suggest Tc^{VII} . More recently, based on rigorous EXAFS fitting, Lukens et al.¹⁶ suggested that the solid is more accurately characterized as Tc_3S_{10} . Synthetic mackinawite (FeS) can also sequester Tc via reduction and coprecipitation,¹⁹ forming phases of which the composition is still uncertain.^{19–21} Although complete understanding of these Tc/S phases is yet to be achieved, preliminary evidence from several studies suggested that Tc sequestered under sulfidic conditions is more recalcitrant to oxidation.^{16,18,21}

Sulfidic conditions in a subsurface environment can be created by either direct injection of H_2S or HS^- or stimulated in situ by microbial sulfate reduction. Injection of H_2S gas has been successfully used to treat Cr(VI)-contaminated sediment,²² but its effectiveness for sequestering Tc at groundwater pHs is low.^{17,23} Stimulating in situ sulfidogenesis is potentially a more environmentally benign (sustainable) approach to this treatment. However, the formation of Tc sulfides along natural redox gradients may be limited by prior (up-gradient or earlier) Tc reduction to $TcO_2 \cdot nH_2O$ under iron reducing conditions. This may also explain why no evidence has been reported for Tc sulfides in naturally developed sulfate reducing sediments.^{13,24} Maximizing the potential for Tc sulfide formation requires a strong reducing agent to rapidly establish sulfidic conditions and thereby minimize the interference from iron reduction.

Emplacing nano zerovalent iron (nZVI) in the presence of sufficient quantities of SO_4^{2-} into the subsurface is a promising approach for achieving these conditions because (i) nZVI will abiotically scavenge alternative electron acceptors (e.g., O_2 and NO_3^-) but not SO_4^{2-} , and (ii) the H_2 generated by Fe^0 dissolution provides an electron donor that is readily utilized by many sulfate reducers.^{25,26} These collateral microbiological effects of nZVI have been frequently documented in both laboratory experiments^{27–30} and pilot- to field-scale applications (i.e., permeable reactive barriers (PRB)).^{31–33} During microbial sulfate reduction, iron sulfides are also expected to form, and these may provide secondary phases—in addition to nZVI—that react with Tc. The most extensively studied iron sulfide phase is nanocrystalline mackinawite (amorphous FeS), commonly considered to be the first iron sulfide phase formed in sulfidic environments.^{34–36} Mackinawite is highly reactive toward various heavy metals,^{37,38} chlorinated solvents,^{39,40} and oxyanions.^{41–43} Therefore, it is expected to play an important role in contaminant degradation/sequestration in sulfidic environments.

The objective of this study was to provide the fundamental geochemical understanding of Tc sequestration during the development of sulfidogenic conditions in the presence of nZVI. Abiotic sulfide was used to simulate biotic sulfate reduction. Figure 1 presents a conceptual model of Tc sequestration pathways in three sequential scenarios: (I) the pre-sulfate reduction stage, (II) the initial stage of sulfate reduction, and (III) the end stage of sulfate reduction. We hypothesized that as sulfate reduction develops, the reactive phases (mineral or aqueous) that are responsible for Tc sequestration evolve, leading to different sequestration pathways and products. By combining wet chemical analysis with electron microscopy, synchrotron X-ray absorption spectroscopy, and other methods, we examined the change of host

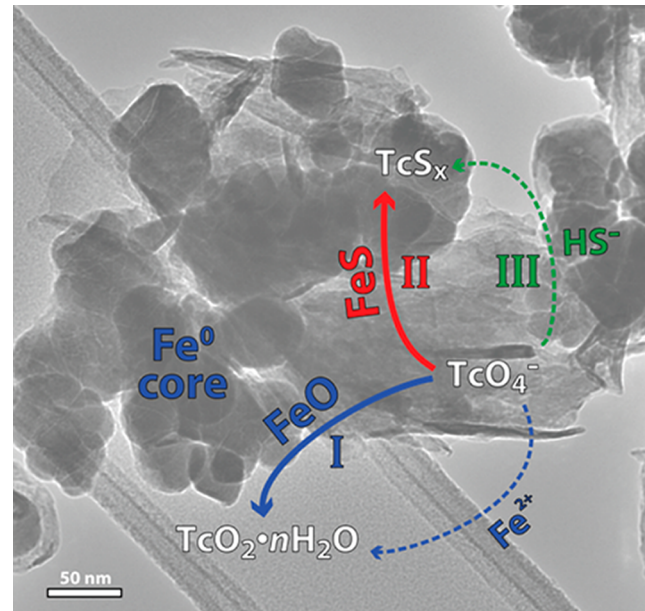


Figure 1. Conceptual model of Tc sequestration pathways under sulfidogenic conditions stimulated by nano zerovalent iron (nZVI). Processes (I), (II), and (III) represent the pre-, initial, and end stages of sulfate reduction, respectively (solid arrows: reaction with mineral phases; dashed arrows: reaction with aqueous species).

mineral phases during sulfidation, Tc sequestration kinetics under incremental S/Fe ratios, and further elucidated sequestration pathways, Tc distribution, phase compositions, and the local coordination environment of Tc within the final Tc–Fe–S solids.

EXPERIMENTAL SECTION

Reagents. $FeCl_3 \cdot 6H_2O$, $NaBH_4$, Na_2S , and methanol were ACS grade. All reagents were used as received without further purification. ^{99}Tc was obtained as concentrated stock solution of ammonium pertechnetate (NH_4TcO_4) from Pacific Northwest National Laboratory. ^{99}Tc is a radioactive beta emitter (half-life 2.13×10^5 years; $E_{max} = 294$ keV) and was handled in a properly equipped radioactive laboratory.

Preparation of nZVI. Sulfur-free nZVI particles were synthesized using a modified version of the borohydride reduction method.⁴⁴ Briefly, $FeCl_3 \cdot 6H_2O$ (2.43 g) was dissolved in 500 mL of 7:3 (v/v) deionized deoxygenated (DI/DO) water/methanol. $NaBH_4$ (1.42 g) was dissolved in 40 mL of DI/DO water and continuously introduced to the $FeCl_3$ solution via a 0.5 mm I.D. plastic tubing with a syringe pump (KD Scientific, Holliston, MA) at 2 mL min^{-1} , while the resulting suspension was vigorously mixed by a homogenizer (Kinematica, Bohemia, NY). After introducing $NaBH_4$, the solution was allowed to sit for 15 min for H_2 bubbles to dissipate. All of the above steps were carried out under an inert gas stream (N_2 or Ar). The suspension was then transferred to an anaerobic chamber (95% N_2 /5% H_2). Solid nZVI particles were recovered by flash drying, as previously described.⁴⁵

Sulfidation. Pre-equilibration between nZVI and sulfide was carried out in 120-mL glass serum bottles. All procedures below were carried out in the anaerobic chamber except where otherwise mentioned. Dry nZVI particles (0.02 g) were weighed into each bottle. The bottles were then filled with 20 mL of deoxygenated Hanford synthetic groundwater

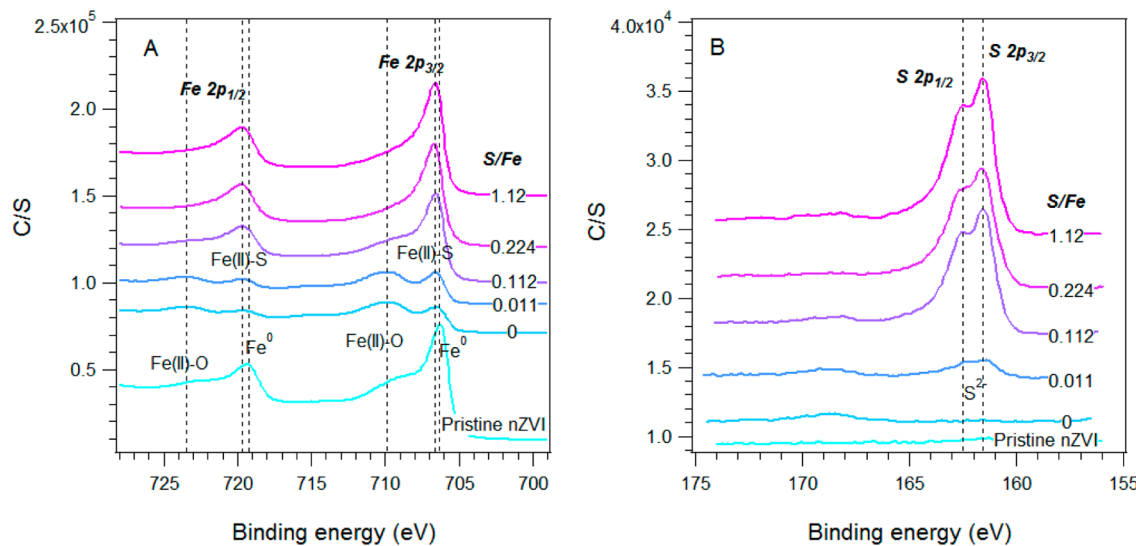


Figure 2. XPS (A) Fe 2p and (B) S 2p narrow region spectra of 0.5 g L⁻¹ nZVI pre-exposed to increasing sulfide concentrations (0–10 mM) for 1 day in HS300 artificial groundwater (Fe peak assignments, represented by dashed lines, were based on literature values summarized by Mullet et al.⁵⁵ and Descotes et al.⁵⁶).

(HS300) buffered at pH 7.9 by 30 mM HEPES (the detailed HS300 recipe is given as Table S1 in the Supporting Information (SI)). The bottles were sonicated in a water bath for 5 min to disperse the nZVI particles. The volume of HS300 was then adjusted up to 100 mL (0.2 g L⁻¹ nZVI). A 0.2 M sulfide stock solution was prepared by dissolving anhydrous Na₂S in deoxygenated HS300 and aliquoted to each bottle to achieve concentrations varying incrementally from 0 to 4 mM, thus providing S/Fe molar ratios ranging from 0 to 1.12. At high sulfide doses, 6 M HCl was added to titrate the pH back to 7.9. The bottles were then sealed with grommet septum stoppers (Bellco Glass, Vineland, NJ), taken out of the anaerobic chamber, and placed in a shaker (150 rpm) at 27 ± 0.5 °C for pre-equilibration, during which time the aqueous sulfide concentration (<0.2 μm) was measured intermittently by the methylene blue colorimetric method (Hach DR700 Spectrophotometer Handbook, Loveland, CO).

Tc Reduction. After 1 day pre-equilibration, 10 mL of nZVI/sulfide suspension was withdrawn from the serum bottle and transferred to a 15-mL serum vial in the anaerobic chamber. TcO₄⁻ stock solution was then added to achieve a final concentration of 6 μM. The reactors were sealed by a 20-mm septum (SUN SRi, Rockwood, TN) and placed on an end-to-end rotator (20 rpm). Tc concentration in the aqueous phase (<0.2 μm) was monitored periodically by liquid scintillation counting (Beckman, Brea, CA). In selected experiments, 0.02-μm filtration was used in order to separate the colloidal phase of Tc from the dissolved phase. Controls included reactors with HS300/Tc but no sulfide, and HS300/Tc with 4 mM sulfide.

Solid Characterization. The bulk mineralogy of sulfidated nZVI was characterized by micro X-ray diffraction (μXRD) and Mössbauer spectroscopy. The near-surface composition of sulfidated nZVI during reaction with different amounts of sulfide was analyzed by X-ray photoelectron spectroscopy (XPS). To recover sufficient quantities of solids for these bulk analyses, 0.5 g L⁻¹ nZVI and proportionally higher sulfide doses (to keep the S/Fe comparable with batch experiments) were used. The microscopic structure of the mineral phase was examined by scanning electron microscopy (SEM) and

transmission electron microscopy (TEM) with energy dispersive X-ray spectroscopy (EDX). For SEM and TEM of Tc-containing samples, lower nZVI (0.2 g L⁻¹ nZVI) and sulfide doses, but higher Tc concentrations (50 μM), were used in order to detect Tc by EDX. Details of these solid phase characterizations are given in SI Section S1.

X-ray Absorption Spectroscopy. Tc K-edge XAS for Tc sequestered by nZVI (0.5 g L⁻¹) and increasing sulfide (0–10 mM) were collected in fluorescence mode at the Stanford Synchrotron Radiation Lightsource (SSRL) on beamline 4-1 and 11-2. EXAFS spectra were analyzed using SixPack, Athena, and Artemis interfaces to the IFEFFIT package.⁴⁶ Back-scattering phase and amplitude functions required for fitting of spectra were obtained from FEFF8.⁴⁷ Details of XAS are given in SI Section S5.

RESULTS AND DISCUSSION

Characterization of Pristine and Sulfidated nZVI. The sulfur-free nZVI particles synthesized by borohydride reduction form chain-like structures, and individual particles have an average diameter of 30–60 nm with a well-defined core–shell structure (SI Figure S1A), both of which are the typical features of nZVI produced by this method.^{48–50} While the core is mainly composed of Fe⁰, the 2–3 nm thick shell appears to be composed of Fe oxides—based on the XPS Fe 2p narrow region spectra (Figure 2A)—and boron, which is evident in the XPS wide survey scans (SI Table S2) and presumably results from the incorporation of iron boride in the outer shell as byproducts during the synthesis.⁵¹ Mössbauer spectroscopic data suggested that the nZVI contains little or no magnetite (Figure 3A), in contrast to nZVI synthesized by H₂ reduction (e.g., RNIP).⁵⁰ Both the μXRD (SI Figure S2A) and Mössbauer spectra of freshly prepared nZVI suggested that the pristine nZVI is largely amorphous. Finally, BET N₂-gas adsorption measurements showed that the material had a surface area of ∼20 m² g⁻¹ which is within the typical range for this type of material.^{48,52}

Sulfidation of nZVI at S/Fe = 0.112 for 1 day resulted in the emergence of poorly crystalline mackinawite phase according to μXRD (SI Figure S2C). The diffraction pattern was slightly

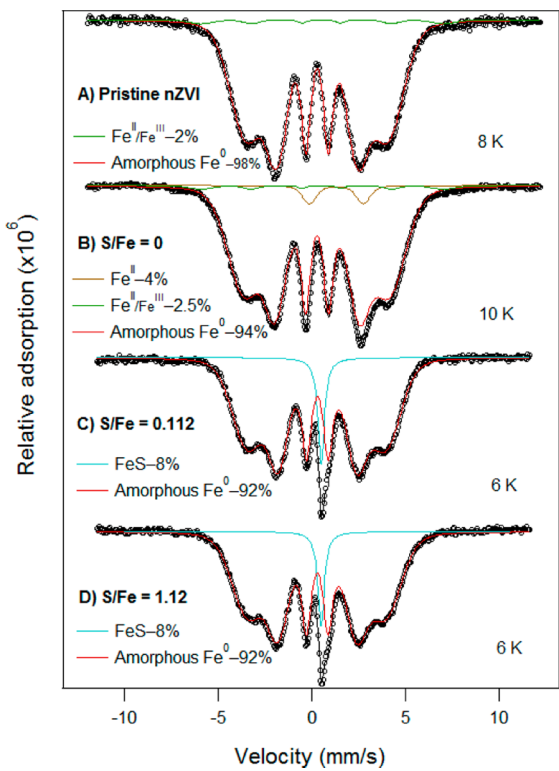


Figure 3. Experimental and modeled Mössbauer spectra of (A) pristine, (B–D) nZVI exposed to 0, 1, and 10 mM sulfide, respectively, in HS300 for 24 h.

different from that observed for bulk crystalline mackinawite, with an expanded *c* parameter that is consistent with disordered or nanocrystalline materials described previously.^{36,53} Mössbauer spectra further confirmed that the bulk phases were mainly composed of residual nZVI (amorphous Fe⁰) and secondary mackinawite (Figure 3). However, fitting the Mössbauer spectra gave a negligible increase in the percentage of mackinawite when S/Fe increased 10-fold from 0.112 to 1.12 (Figure 3). Likewise, XPS wide survey scans showed the surface atomic ratio of sulfide leveling off at S/Fe \geq 0.112 (SI Table S2). The inhibition of sulfide uptake was further confirmed by significant aqueous sulfide detected at S/Fe = 0.224 and 0.56

even after extended exposure time (SI Figure S3). This is likely caused by a decrease in available Fe/FeO surface sites due to the formation of FeS, which is evidenced by the attenuation of broad Fe(II)–O peaks around 710 and 723 eV and evolution of sharp Fe(II)–S peaks around 706 and 719 eV when S/Fe increased from 0 to 0.112 in the XPS narrow region spectra of Fe 2p (Figure 2A). Note that the overlap of Fe(0) and Fe(II)–S peaks prevents quantifying these two species separately, but parallel S 2p spectra confirmed that the enhanced peaks were largely due to the formation of FeS (Figure 2B). Alternatively, particle aggregation—either originating with pristine nZVI or further induced by sulfidation—may also decrease the availability of surface sites to react with sulfide, and thereby possibly contribute to limiting sulfide uptake. This effect has been reported to significantly suppress sulfide uptake by aggregated Ag nanoparticles (NPs) relative to well-dispersed NPs.⁵⁴ TEMs of nZVI sulfidated at S/Fe = 0.112 revealed that FeS deposition onto the surfaces of nZVI appears to be highly nonuniform and does not leave a well-defined Fe⁰/FeS core–shell structure. Instead, a laminar phase appears to grow out of the original nZVI particles, forming distinct phases that are closely associated with material retaining the original nZVI structure. The chemical composition and diffraction pattern further confirmed that this phase is FeS (SI Figure S1C).

Tc Sequestration Kinetics. Aqueous TcO₄⁻ was rapidly removed from solution at all values of S/Fe except 0 and 1.12 (Figure 4A). However, the kinetics of this reaction were not entirely pseudo-first-order because of tailing that appears to approach a limiting value after \sim 1 h. Therefore, the TcO₄⁻ removal rates were quantified using only the initial, linear portion of the ln (concentration) vs time plots. Figure 4B shows the initial Tc immobilization rate (left axis) and residual sulfide concentration measured before Tc addition (right axis) vs S/Fe in each experiment. As S/Fe increased from 0 to 0.045, the Tc disappearance rate increased. The reaction rate was too fast to be accurately determined from the data obtained at S/Fe = 0.056 and 0.224, but higher values of S/Fe resulted in decreased Tc removal rates. The high Tc removal rate observed at low S/Fe ratios can be explained by either enhanced nZVI corrosion due to sulfide facilitated corrosion⁵⁷ and/or increasing formation of reactive FeS. Both of these two mechanisms have been invoked to explain the enhanced

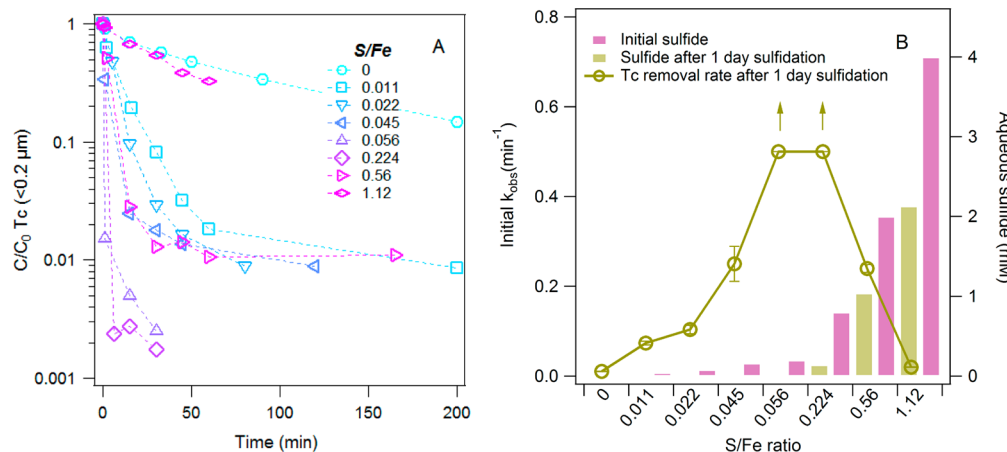


Figure 4. (A) Tc reduction kinetics at increasing S/Fe ratios after 1 day pre-exposure of nZVI to sulfide ($n = 2$). (B) Aqueous sulfide concentrations and initial Tc removal rate constants after 1 day pre-exposure of nZVI to various concentrations of sulfide (error bars represent standard deviations from linear regression; upward arrows represent lower limits because the reduction rate was too fast to be determined from the data).

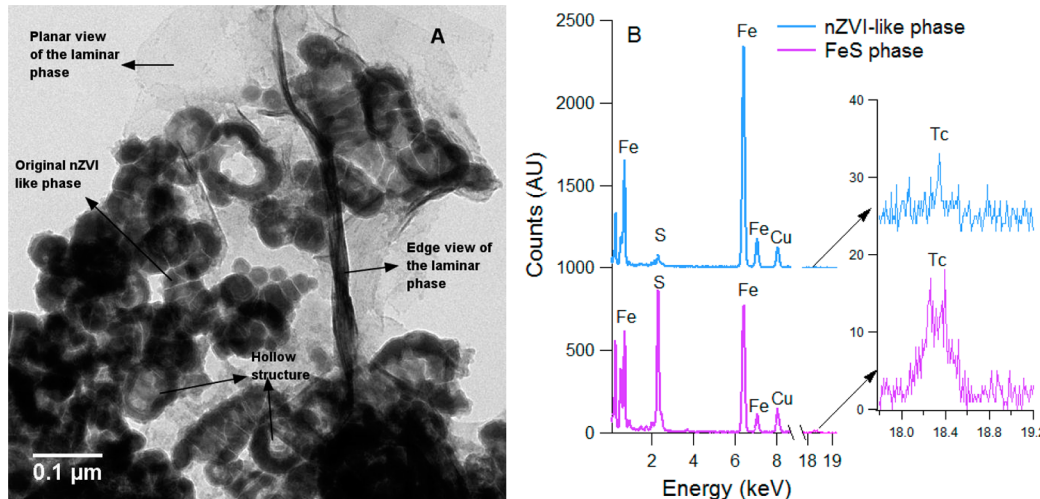


Figure 5. (A) Transmission electron micrograph of sulfidated nZVI exposed to TcO_4^- . (B) Representative EDX spectra of Fe-rich and S-rich area with enlarged spectra showing Tc ($[\text{nZVI}] = 0.2 \text{ g L}^{-1}$; $[\text{S}^{2-}] = 0.4 \text{ mM}$).

reactivity of sulfidated ZVI with chlorinated solvents (e.g., carbon tetrachloride and trichloroethylene).^{28,39,58} In the present study, however, the latter mechanism is considered more likely because mackinawite has been shown to be a highly reactive phase with a wide range of inorganic oxyanions, including TcO_4^- . This hypothesis is also backed by the correlation between enhanced Tc removal rate and the increasing amount of surface FeS observed by XPS (Figure 2) as S/Fe increased from 0 to 0.112. Further evidence for this interpretation is provided by the XAS data presented below.

At high S/Fe, the inhibition of Tc removal varies with the residual aqueous sulfide concentration. As S/Fe increased from 0.224 to 1.12, the reaction rate decreased significantly while the aqueous sulfide concentration increased from ~0.2 to ~2 mM (Figure 4B), indicating that the inhibition is likely caused by aqueous sulfide. To verify this, additional experiments were performed that showed removal of excess aqueous sulfide before Tc addition restored faster Tc removal (SI Figure S5). Inhibition by sulfide has been previously observed for adsorption of molybdate onto pyrite (FeS_2),⁵⁹ which was interpreted as a result of sulfide competing for adsorption sites and/or the formation of Mo–S complexes. Direct interaction between TcO_4^- and aqueous sulfide has been reported to form Tc_2S_7 (or Tc_3S_{10}) solids at acidic or basic pHs.^{17,23} However, at neutral pHs similar to our experimental conditions, it was found that Tc removal—in a way that is consistent with our observations—was negligible.^{17,23}

We note that these studies quantified “aqueous Tc” by measuring Tc in either supernatant after centrifugation²³ or 0.45-μm filtrate,¹⁷ both of which may not be sufficient to differentiate truly dissolved TcO_4^- from colloidal Tc_2S_7 .⁶⁰ To test this, we compared Tc concentration after 0.2- and 0.02-μm filtration when TcO_4^- was reacted with 0 and 4 mM sulfide (SI Figure S6). In the absence of sulfide, Tc activity was kept unchanged in 0.2-μm filtrate and only slightly decreased in 0.02-μm filtrate after 96 h reaction. By contrast, in the presence of 4 mM sulfide, Tc activity decreased by 15% in 0.2-μm filtrate and by 35% in 0.02-μm filtrate, which indicates the formation and growth of Tc sulfide, most likely Tc_2S_7 , colloids. However, it is worth noting that the time required to form significant quantities of colloidal Tc is considerably longer than the batch reaction time presented in Figure 4A. Therefore, the

contributions of this reaction to the overall TcO_4^- removal, even at high S/Fe, might be limited, and the possibility that other factors contributed to the observed inhibition of Tc removal, such as sulfide competing for reaction sites, cannot be excluded.

Microscopy. The Tc distribution between the mineral phases was examined by TEM at S/Fe = 0.112. This ratio was chosen for two reasons. (i) Characterizations on sulfidated nZVI suggest that at S/Fe = 0.112, a significant amount of FeS is formed, but it is still much less abundant than residual nZVI phases. In addition, the majority of nZVI is not occluded by FeS coating (therefore, if FeS is indeed more important for Tc sequestration, as indicated by kinetic data, Tc should be partitioned preferentially to FeS). (ii) At S/Fe = 0.112, no excess aqueous sulfide was present (SI Figure S3), and therefore interference by reaction between Tc and HS^- was minimized. Figure 5A shows the morphology of sulfidated nZVI after reacting with TcO_4^- . Consistent with microscopy on sulfidated nZVI that was not reacted with Tc (SI Figure S1C), two morphologically distinct phases were present: aggregated particles that retain structure similar to pristine nZVI and a laminar phase that is most likely mackinawite. A third type of structure that was frequently encountered, but not observed in samples without Tc, was the hollow structures. Similar looking structures have been observed when Cu^0 NPs transform to sulfide-deficient Cu_xS NPs under bench-simulated sulfate reducing conditions.⁶¹ Dispersed copper sulfide NPs that are more sulfide-rich were also observed. The authors suggested that the hollow structures might be a result of direct transformation of the zerovalent metal NPs due to a counter-diffusion phenomenon known as nanoscale Kirkendall effect,⁶² whereas the dispersed NPs probably form by aqueous phase precipitation. Similar mechanisms might apply in the present study, given that the EDX spectra suggest that the laminar phase is more sulfide-rich than the hollow particles (data not shown). The absence of the hollow structures in the samples not exposed to Tc might be related to the lack of “aging” (Tc samples were kept in aqueous suspension for 2 months before being prepared for TEM, whereas samples without Tc were recovered as solid powder immediately after 1 day of sulfidation).

Despite the highly heterogeneous morphology formed upon nZVI sulfidation, Tc appears to be mainly associated with the FeS phase. Figure 5B shows the representative EDX spectra for nZVI-like and FeS phases. It can be seen that the FeS phase contains substantially more Tc than the nZVI-like phase. Although the level of Tc in the FeS phase was found to vary, up to 4% of Tc (atomic ratio) was detected in several locations. The preferential association of Tc with FeS further supports the hypothesis that FeS formed during sulfidation is mainly responsible for the increasing trend in Tc removal rates observed at low S/Fe ratios.

X-ray Absorption Spectroscopy. To better characterize the state of the sequestered Tc, Tc K-edge XAS data were obtained on solids recovered for each S/Fe ratio. The XANES spectra did not show the diagnostic pre-edge peak of TcO_4^- in any of the samples, suggesting that TcO_4^- was reduced to below detection. The Tc absorption edge decreased steeply from ca. 21.060 to ca. 21.054 keV as S/Fe increased from 0 to 0.056, but gradually leveled off above 0.056 (Figure 6). Given

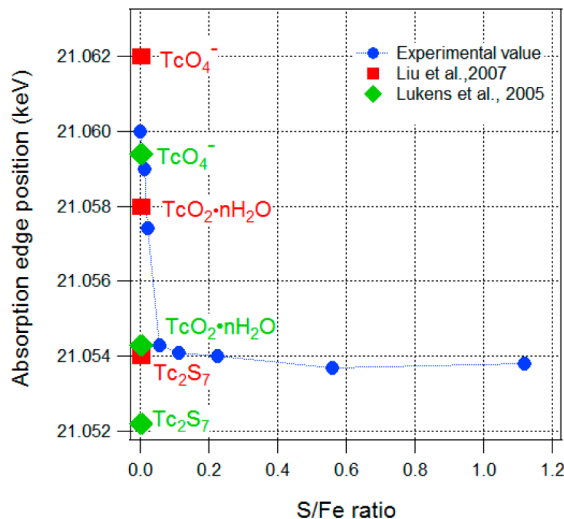


Figure 6. Tc K-edge adsorption edge position of Tc immobilized at incremental S/Fe ratios (blue solid dots) vs the first inflection point of TcO_4^- , TcO_2 , and Tc_2S_7 reported in previous studies^{16,18} (TcS_2 is not included because TcS_2 was reported only in Wharton et al.²¹ and the value of its edge position (and the values of other comparable Tc compounds) is about 20 eV lower than values reported in other studies).

that the position of Tc K-edge absorption edge does not always correspond to the oxidation state of this element^{63,64} and Tc_2S_7 has been reported to have a lower adsorption edge than TcO_2 ,^{16,18} this two-phase trend most likely reflects changes in Tc speciation rather than its oxidation state. This interpretation is further supported by the EXAFS data in Figure 7, which shows a clear progression of Tc speciation from one pattern to the other with increasing S/Fe. The shell-by-shell EXAFS fit was further conducted for Tc reduced at S/Fe = 0 and 1.12, respectively, as two end-members (at S/Fe = 1.12, we only consider the speciation of Tc reacted with mineral phases because the contribution from colloidal Tc to the overall speciation of reduced Tc is small). The fitting results are summarized in SI Table S4. In the absence of sulfide, Tc has an inner shell coordination with 6 O atoms at a distance of 2.02 Å, which agrees well with the structure of $\text{Tc}^{IV}\text{O}_2\cdot n\text{H}_2\text{O}$. Different from previously reported EXAFS fit for Tc reduced by different

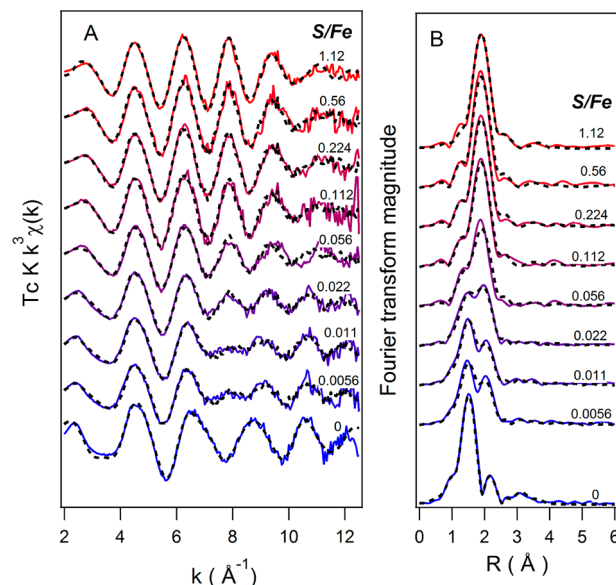


Figure 7. (A) Tc K-edge EXAFS and (B) the respective Fourier transform of Tc reduced at increasing S/Fe ratios. Experimental data are represented with circles. Fits are shown as solid lines (shell-by-shell fit for S/Fe = 0 and 1.12 and linear combination fit for all other S/Fe ratios in-between).

nZVI under simulated waste conditions,⁶⁵ the best fit to our data was obtained with Tc (instead of Fe) as neighboring metal atoms in the second shell. At S/Fe = 1.12, Tc is surrounded by 6 S atoms, 2 at 2.30 Å and the other 4 at 2.47 Å. The fit is similar to the crystallographic data for TcS_2 ,⁶⁶ although the S coordination number and distance are not entirely consistent. Compared with previous studies on Tc speciation after reacting with synthetic FeS, our finding generally agrees with the TcS_2 -like phases reported by Wharton et al.²¹ but not the $\text{TcO}_2\cdot n\text{H}_2\text{O}$ reported by Liu et al.¹⁹ The reason for the inconsistency requires further investigation, but likely involves the high loading of TcO_4^- used by Liu et al. (150 μM) and differences in the surface properties of FeS.

By taking the two spectra at S/Fe = 0 and 1.12 as principal components (or “end-members”), the relative proportions of $\text{TcO}_2\cdot n\text{H}_2\text{O}$ to TcS_2 can be estimated by linear combination fitting (LCF) to the EXAFS spectra of different S/Fe ratios (Figure 7). Figure 8 plots the LCF results at incremental S/Fe ratios. As S/Fe increased, the portion of the high S/Fe end-member (TcS_2) generally increased while the portion of low S/Fe end-member ($\text{TcO}_2\cdot n\text{H}_2\text{O}$) decreased. At S/Fe = 0.011, about one-third of the reduced Tc speciation can be accounted for by the TcS_2 , despite only trace amounts of surface FeS detected by XPS (Figure 2A). Taken together, these data suggest that FeS has a higher affinity for TcO_4^- than do nZVI/Fe oxides. In light of this result, it is noteworthy that the most substantial change in Tc speciation (by EXAFS)—the steep drop in the Tc absorption edge (by XANES)—occurred concurrently with the rapid increase of initial Tc removal rates at low S/Fe ratios. The agreement between the XAS and kinetic data again supports the conclusion that the increasing Tc removal rate during the initial stage of sulfidation is due to the rapid shift of Tc sequestration pathway from reduction by nZVI to reduction by FeS (Figure 1). As sulfidation proceeds, surface FeS apparently becomes the dominant mineral phase for Tc sequestration because Tc EXAFS spectra from above S/Fe = 0.112 were nearly identical to the high S/Fe end-member.

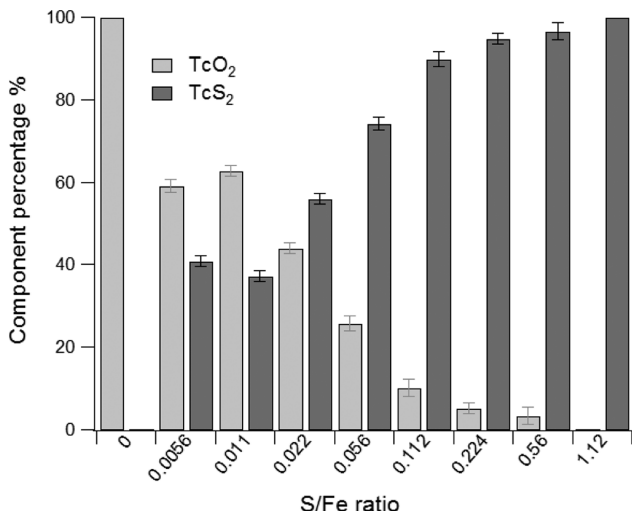


Figure 8. Tc speciation at different S/Fe ratios based on linear combination fitting of Tc EXAFS (Figure 7) using the spectra at S/Fe = 0 and 1.12 as two end-members.

Implications for Tc Sequestration in the Subsurface. The results presented here demonstrate that sulfidation of nZVI, although forming highly heterogeneous mineral surfaces, can direct TcO_4^- sequestration products from Tc^{IV} oxide (pathway I in Figure 1) to Tc^{IV} sulfide phases (pathway II in Figure 1) under groundwater conditions. Given the typically low TcO_4^- concentration in groundwater (even as a contaminant $<10^{-5}$ M), and that TcO_4^- has a higher affinity for FeS, it can be expected that sulfidic conditions will favor sequestration of Tc as Tc sulfides rather than Tc oxides, even at the early stage of microbial sulfate reduction. Other reducing iron phases—such as residual nZVI or secondary Fe(II) minerals formed from reaction of nZVI with groundwater constituents—reduce TcO_4^- readily, but nevertheless are outcompeted by FeS. As sulfate reduction proceeds, these iron phases (and possibly other naturally abundant Fe oxide minerals) will undergo further sulfidation to provide additional FeS capacity for Tc sequestration. At the same time, the formation of iron sulfides will lower the free aqueous sulfide concentration, thereby decreasing the possibility of forming potentially mobile colloidal Tc sulfide phases (pathway III in Figure 1).

In contrast to conventional (n)ZVI applications, where the Fe^0 directly reduces target contaminants, this study demonstrates a scenario where the main goal of adding nZVI is conditioning and sustaining a sufficiently reducing environment to favor microbial sulfate reduction. In actual remedial practice, however, direct reduction of TcO_4^- to TcO_2 by nZVI could be the dominant sequestration pathway before microbial sulfate reduction is established (pathway I in Figure 1). Additional EXAFS spectra showed that Tc reduced by nZVI and then exposed to 1 mM sulfide for 3 days is nearly identical to Tc reduced under $S/\text{Fe} = 0.011$ (SI Figure S11), indicating partial transformation from $\text{TcO}_2 \cdot n\text{H}_2\text{O}$ to TcS_2 . The rate of transformation, however, is considerably slower than the kinetics of Tc removal shown in Figure 4, even though geochemical modeling indicated that the transformation is thermodynamically possible (SI Figure S12). Therefore, field-scale application of nZVI for the remediation of Tc may require some direct introduction of sulfide to minimize the initial formation of TcO_2 , such as by pretreating nZVI with aqueous

sulfide. This study shows that a small amount of added sulfide may be sufficient to alter the dominant sequestration pathway, and at the same time, not substantially inhibit the ability of the nZVI to condition the subsurface to a sufficiently reducing environment.

There are many additional uncertainties to be addressed before up-scaling such a remediation strategy, including how to effectively deliver nZVI in the subsurface environment,⁶⁷ the effects of physical heterogeneity of the subsurface on Tc sequestration, and the effects of interactions between Tc and natural organic matter (especially thiol moieties) on Tc sequestration in sulfidic environments.⁶⁸ Many of these topics have been examined previously or are under investigation currently, but are beyond the scope of this study. Regardless, the present study suggests an effective alternative for Tc sequestration.

ASSOCIATED CONTENT

Supporting Information

Details on the characterization and properties of original and sulfidated nZVI, batch Tc reduction kinetics under high Fe dose, evidence of formation of colloidal Tc phases, additional SEM/TEM results of solids exposed to Tc, additional XAS information, and geochemical speciation modeling for Fe/S/Tc under relevant groundwater conditions. This material is available free of charge via the Internet at <http://pubs.acs.org>.

AUTHOR INFORMATION

Corresponding Author

*E-mail: tratnyek@ebs.ogi.edu; phone: 503-748-1023; fax: 503-748-1464.

Present Address

[†]School of Earth Sciences, Environmental Earth System Science Department, Stanford University Stanford, CA, 94305-4216.

Notes

The authors declare no competing financial interest.

ACKNOWLEDGMENTS

This material is based on work supported by the Subsurface Biogeochemical Research Program of the U.S. Department of Energy, Award DE-SC0001376. This report has not been subject to review by the DOE and therefore does not necessarily reflect agency views and no official endorsements should be inferred. Mössbauer, XPS, μ XRD, SEM, and TEM/EDS were performed using the Environmental Molecular Sciences Laboratory (EMSL), a national scientific user facility sponsored by the Department of Energy's Office of Biological and Environmental Research and located at Pacific Northwest National Laboratory. XAS was carried out at the Stanford Synchrotron Radiation Lightsource, a Directorate of SLAC National Accelerator Laboratory and an Office of Science User Facility operated for the U.S. Department of Energy Office of Science by Stanford University. We thank Alice Dohnalkova and Charles Resch for EM sample preparation, Sung-Woo Lee for preliminary XAS data collection and discussion, Ninian Blackburn for fitting preliminary XAS data, Danielle Jansik and James Szecsody for general discussions, and Wayne Lukens for providing XAS spectra for Tc model compounds and advice regarding the XAS fitting.

■ REFERENCES

- (1) Hartman, M.; Barnett, D.; Chou, C. et al. *Hanford Site Groundwater Monitoring for Fiscal Year 1999*; PNNL-12086; Pacific Northwest National Laboratory: Richland, WA, 2000.
- (2) Jones, T. E.; Khaleel, R.; Myers, D. A.; Shade, J. W.; Wood, M. I. *A Summary and Evaluation of Hanford Site Tank Farm Subsurface Contamination*; HNF-2603; Lockheed Martin Hanford: Richland, WA, 1998.
- (3) Beasley, T. M.; Dixon, P. R.; Mann, L. J. ^{99}Tc , ^{236}U , and ^{237}Np in the Snake river plain aquifer at the Idaho National Engineering and Environmental Laboratory, Idaho Falls, Idaho. *Environ. Sci. Technol.* **1998**, *32*, 3875–3881.
- (4) Haase, C.; Dreier, R.; McMaster, W.; Moore, G.; Solomon, D. Characteristics and modes of occurrence of groundwater contaminants on the U.S. Department of Energy reservation in Oak Ridge, Tennessee. *Geo. Soc. Am. Abs.* **1991**, *23*, 7–77.
- (5) Maes, A.; Geraedts, K.; Bruggeman, C.; Vancluysen, J.; Rossberg, A.; Hennig, C. Evidence for the interaction of technetium colloids with humic substances by X-ray absorption spectroscopy. *Environ. Sci. Technol.* **2004**, *38*, 2044–2051.
- (6) Rard, J. A. Current status of the thermodynamic data for technetium and its compounds and aqueous species. *J. Nucl. Radiochem. Sci.* **2005**, *6*, 197–204.
- (7) Icenhower, J. P.; Qafoku, N. P.; Zachara, J. M.; Martin, W. J. The biogeochemistry of technetium: A review of the behavior of an artificial element in the natural environment. *Am. J. Sci.* **2010**, *310*, 721–752.
- (8) O'Loughlin, E. J.; Boyanov, M. I.; Antonopoulos, D. A.; Kemner, K. M. Redox processes affecting the speciation of technetium, uranium, neptunium, and plutonium in aquatic and terrestrial environments. In *Aquatic Redox Chemistry*; Tratnyek, P. G., Grundl, T. J., Haderlein, S. B., Eds.; American Chemical Society: Washington, DC, 2011; ACS Symposium Series Vol. 1071, pp 477–517.
- (9) Cui, D.; Eriksen, T. E. Reduction of pertechnetate in solution by heterogeneous electron transfer from Fe(II)-containing geological material. *Environ. Sci. Technol.* **1996**, *30*, 2263–2269.
- (10) Peretyazhko, T.; Zachara, J. M.; Heald, S. M.; Jeon, B.-H.; Kukkadapu, R. K.; Liu, C.; Moore, D.; Resch, C. T. Heterogeneous reduction of Tc(VII) by Fe(II) at the solid-water interface. *Geochim. Cosmochim. Acta* **2009**, *72*, 1521–1539.
- (11) Plymale, A. E.; Fredrickson, J. K.; Zachara, J. M.; Dohnalkova, A. C.; Heald, S. M.; Moore, D. A.; Kennedy, D. W.; Marshall, M. J.; Wang, C.; Resch, C. T.; Nachimuthu, P. Competitive reduction of pertechnetate ($^{99}\text{TcO}_4^-$) by dissimilatory metal reducing bacteria and biogenic Fe (II). *Environ. Sci. Technol.* **2011**, *45*, 951–957.
- (12) Zachara, J. M.; Heald, S. M.; Jeon, B.; Kukkadapu, R. K.; Liu, C.; McKinley, J. P.; Dohnalkova, A. C.; Moore, D. A. Reduction of pertechnetate [Tc(VII)] by aqueous Fe(II) and the nature of solid phase redox products. *Geochim. Cosmochim. Acta* **2007**, *71*, 2137–2157.
- (13) Burke, I. T.; Boothman, C.; Lloyd, J. R.; Mortimer, R. J. G.; Livens, F. R.; Morris, K. Effects of progressive anoxia on the solubility of technetium in sediments. *Environ. Sci. Technol.* **2005**, *39*, 4109–4116.
- (14) McBeth, J. M.; Lear, G.; Lloyd, J. R. Technetium reduction and reoxidation in aquifer sediments. *Geomicrobiol. J.* **2007**, *24*, 189–197.
- (15) Um, W.; Chang, H.; Icenhower, J. P.; Lukens, W. W.; Serne, R. J.; Qafoku, N. P.; Westsik, J., J. H.; Buck, E. C.; Smith, S. C. Immobilization of 99-technetium (VII) by Fe(II)-goethite and limited reoxidation. *Environ. Sci. Technol.* **2011**, *45*, 4904–4913.
- (16) Lukens, W. W.; Bucher, J. J.; Shuh, D. K.; Edelstein, N. M. Evolution of technetium speciation in reducing grout. *Environ. Sci. Technol.* **2005**, *39*, 8064–8070.
- (17) Kunze, S.; Neck, V.; Gompper, K.; Fanganel, T. Studies on the immobilization of technetium under near field geochemical conditions. *Radiochim. Acta* **1996**, *74*, 159–163.
- (18) Liu, Y.; Terry, J.; Jurrison, S. Pertechnetate immobilization in aqueous media with hydrogen sulfide under anaerobic and aerobic environments. *Radiochim. Acta* **2007**, *95*, 717–725.
- (19) Liu, Y.; Terry, J.; Jurrison, S. Pertechnetate immobilization with amorphous iron sulfide. *Radiochim. Acta* **2008**, *96*, 823–833.
- (20) Watson, J. H. P.; Croudace, I. W.; Warwick, P. E.; James, P. A. B.; Charnock, J. M.; Ellwood, D. C. Adsorption of radioactive metals by strongly magnetic iron sulfide nanoparticles produced by sulfate-reducing bacteria. *Sep. Sci. Technol.* **2001**, *36*, 2571–2607.
- (21) Wharton, M. J. A. B.; Charnock, J. M.; Livens, F. R.; Patrick, R. A. D.; Collision, D. An X-ray absorption spectroscopy study of the coprecipitation of Tc and Re with mackinawite (FeS). *Appl. Geochem.* **2000**, *15*, 347–354.
- (22) Thornton, E. C.; Amonette, J. E. Hydrogen sulfide gas treatment of Cr(VI)-contaminated sediment samples from a plating-waste disposal site: Implications for in-situ remediation. *Environ. Sci. Technol.* **1999**, *33*, 4096–4101.
- (23) Liu, Y.; Terry, J.; Jurrison, S. Pertechnetate immobilization in aqueous media with hydrogen sulfide under anaerobic and aerobic environments. *Radiochim. Acta* **2007**, *95*, 717–725.
- (24) Keith-Roach, M. J.; Morris, K.; Dahlgaard, H. An investigation into technetium binding in sediments. *Mar. Chem.* **2003**, *81*, 149–162.
- (25) Scherer, M. M.; Richter, S.; Richard, L. V.; Alvarez, P. J. Chemistry and microbiology of permeable reactive barriers for in situ groundwater clean up. *Crit. Rev. Environ. Sci. Technol.* **2000**, *30*, 363–411.
- (26) Liamleam, W.; Annachhatre, A. Electron donors for biological sulfate reduction. *Biotechnol. Adv.* **2007**, *25*, 452–463.
- (27) Gu, B.; Phelps, T. J.; Liang, L.; Dickey, M. J.; Roh, Y.; Kinsall, B. L.; Palumbo, A. V.; Jacobs, G. K. Biogeochemical dynamics in zero-valent iron columns: Implications for permeable reactive barriers. *Environ. Sci. Technol.* **1999**, *33*, 2170–2177.
- (28) Van Nooten, T.; Lieben, F.; Dries, J.; Pirard, E.; Springael, D.; Bastiaens, L. Impact of microbial activities on the mineralogy and performance of column-scale permeable reactive iron barriers operation under two different conditions. *Environ. Sci. Technol.* **2007**, *41*, 5274–5230.
- (29) Kirschling, T. L.; Gregory, K. B.; Minkley, E. G., Jr.; Lowry, G. V.; Tilton, R. D. Impact of nanoscale zero valent iron on geochemistry and microbial populations in trichloroethylene contaminated aquifer materials. *Environ. Sci. Technol.* **2010**, *44*, 3474–3480.
- (30) Van Nooten, T.; Springael, D.; Bastiaens, L. Positive impact of microorganisms on the performance of laboratory-scale permeable reactive iron barriers. *Environ. Sci. Technol.* **2008**, *42*, 1680–1686.
- (31) Van Nooten, T.; Springael, D.; Bastiaens, L. Microbial community characterization in a pilot-scale permeable reactive iron barrier. *Environ. Eng. Sci.* **2010**, *27*, 287–292.
- (32) Phillips, D. H.; Van Nooten, T.; Bastiaens, L.; Russell, M. I.; Dickson, K.; Plant, S.; Ahad, J. M. E.; Newton, T.; Elliot, T.; Kalin, R. M. Ten year performance evaluation of a field-scale zero-valent iron permeable reactive barrier installed to remediate trichloroethylene contaminated groundwater. *Environ. Sci. Technol.* **2010**, *44*, 3861–3869.
- (33) Gu, B.; Watson, D. B.; Wu, L.; Phillips, D. H.; White, D. C.; Zhou, J. Microbiological characteristics in a zero-valent iron reactive barrier. *Environ. Monit. Assess.* **2002**, *77*, 293–309.
- (34) Morse, J. W.; Millero, F. J.; Cornwell, J. C.; Rickard, D. The chemistry of the hydrogen sulfide and iron sulfide systems in natural waters. *Earth-Sci. Rev.* **1987**, *24*, 1–42.
- (35) Rickard, D.; Luther, G. W., III Chemistry of iron sulfides. *Chem. Rev.* **2007**, *107*, 514–562.
- (36) Jeong, H. Y.; Lee, J. H.; Hayes, K. F. Characterization of synthetic nanocrystalline mackinawite: Crystal structure, particle size and specific surface area. *Geochim. Cosmochim. Acta* **2008**, *72*, 493–505.
- (37) Jeong, H. Y.; Sun, K.; Hayes, K. F. Microscopic and spectroscopic characterization of Hg(II) immobilization by mackinawite. *Environ. Sci. Technol.* **2010**, *44*, 7476–7683.
- (38) Coles, C. A.; Rao, S. R.; Yong, R. N. Lead and cadmium interactions with mackinawite: Retention mechanisms and the role of pH. *Environ. Sci. Technol.* **2000**, *34*, 996–1000.

- (39) Bulter, E. C.; Hayes, K. F. Factors influencing rates and products in the transformation of trichloroethylene by iron sulfide and iron metal. *Environ. Sci. Technol.* **2001**, *35*, 3884–3891.
- (40) He, Y. T.; Wilson, J. T.; Wilkin, R. T. Impact of iron sulfide transformation on trichloroethylene degradation. *Geochim. Cosmochim. Acta* **2010**, *74*, 2025–2039.
- (41) Scheinost, A. C.; Charlet, L. Selenite reduction by mackinawite, magnetite and siderite: XAS characterization of nanosized redox products. *Environ. Sci. Technol.* **2008**, *42*, 1984–1989.
- (42) Hyun, S. P.; Davis, J. A.; Sun, K.; Hayes, K. F. Uranium(VI) reduction by iron(II) monosulfide mackinawite. *Environ. Sci. Technol.* **2012**, *46*, 3369–3376.
- (43) Wolthers, M.; Charlet, L.; Van Der Weijden, C. H.; Van Der Linde, P. R.; Rickard, D. Arsenic mobility in the ambient sulfidic environment: sorption of arsenic(V) and arsenic(III) onto disordered mackinawite. *Geochim. Cosmochim. Acta* **2005**, *69*, 3483–3492.
- (44) Wang, C.; Zhang, W. Synthesizing nanoscale iron particles for rapid and complete dechlorination of TCE and PCBs. *Environ. Sci. Technol.* **1997**, *31*, 2154–2156.
- (45) Nurmi, J.; Sarathy, V.; Tratnyek, P.; Baer, D.; Amonette, J.; Karkamkar, A. Recovery of iron/iron oxide nanoparticles from solution: Comparison of methods and their effects. *J. Nanopart. Res.* **2011**, *13*, 1937–1952.
- (46) Ravel, B.; Newville, M. ATHENA, ARTEMIS, HEPHAESTUS: Data analysis for X-ray absorption spectroscopy using IFEFFIT. *J. Synchrotron Radiat.* **2005**, *12*, 537–541.
- (47) Rehr, J. J.; Albers, R. C.; Zabinsky, S. I. High-order multiple-scattering calculations of X-ray-absorption fine structure. *Phys. Rev. Lett.* **1992**, *69*, 3397–3400.
- (48) Li, X.-Q.; Elliott, D. W.; Zhang, W.-X. Zero-valent iron nanoparticles for abatement of environmental pollutants: Materials and engineering aspects. *Crit. Rev. Solid State Mater. Sci.* **2006**, *31*, 111–122.
- (49) Baer, D. R.; Tratnyek, P. G.; Qiang, Y.; Amonette, J. E.; Linehan, J.; Sarathy, V.; Nurmi, J. T.; Wang, C.; Anthony, J. Synthesis, characterization, and properties of zero-valent iron nanoparticles. In *Environmental Applications of Nanomaterials: Synthesis, Sorbents, and Sensors*; Fryxell, G. E., Ed.; Imperial College Press: London, 2007; pp 49–86.
- (50) Nurmi, J. T.; Tratnyek, P. G.; Sarathy, V.; Baer, D. R.; Amonette, J. E.; Pecher, K.; Wang, C.; Linehan, J. C.; Matson, D. W.; Penn, R. L.; Driessens, M. D. Characterization and properties of metallic iron nanoparticles: Spectroscopy, electrochemistry, and kinetics. *Environ. Sci. Technol.* **2005**, *39*, 1221–1230.
- (51) Glavee, G. N.; Klabunde, K. J.; Sorensen, C. M.; Hadjipanayis, G. C. Chemistry of borohydride reduction of iron(II) and iron(III) ions in aqueous and nonaqueous media - Formation of nanoscale Fe, FeB, and Fe₂B powders. *Inorg. Chem.* **1995**, *34*, 28–35.
- (52) Wang, Q.; Snyder, S.; Kim, J.; Choi, H. Aqueous ethanol modified nanoscale zerovalent iron in bromate reduction: Synthesis, characterization, and reactivity. *Environ. Sci. Technol.* **2009**, *43*, 3292–3299.
- (53) Wolthers, M.; Van der Gaast, S. J.; Rickard, D. The structure of disordered mackinawite. *Am. Mineral.* **2003**, *88*, 2007–2015.
- (54) Reinsch, B. C.; Levard, C.; Li, Z.; Ma, R.; Wise, A.; Gregory, K. B.; Brown, G. E.; Lowry, G. V. Sulfidation of silver nanoparticles decreases *Escherichia coli* growth inhibition. *Environ. Sci. Technol.* **2012**, *46*, 6992–7000.
- (55) Mullet, M.; Boursiquot, S.; Abdelmoula, M.; Genin, J.; Ehrhardt, J. Surface chemistry and structural properties of mackinawite prepared by reaction of sulfide ions with metallic iron. *Geochim. Cosmochim. Acta* **2002**, *66*, 829–836.
- (56) Descotes, M.; Mercier, F.; Thromat, N.; Beaucaire, C.; Gautier-Soyer, M. Use of XPS in the determination of chemical environment and oxidation state of iron and sulfur samples: Constitution of a data basis in binding energies for Fe and S reference compounds and applications to the evidence of surface species of an oxidized pyrite in a carbonate medium. *Appl. Surf. Sci.* **2000**, *165*, 288–302.
- (57) Turcio-Ortega, D.; Fan, D.; Tratnyek, P. G.; Kim, E.-J.; Chang, Y.-S. Reactivity of Fe/FeS nanoparticles: Electrolyte composition effects on corrosion electrochemistry. *Environ. Sci. Technol.* **2012**, *46*, 12484–12492.
- (58) Kim, E.-J.; Kim, J.-H.; Azad, A.-M.; Chang, Y.-S. Facile synthesis and characterization of Fe/FeS nanoparticles for environmental applications. *ACS Appl. Mater. Interfaces* **2011**, *3*, 1457–1462.
- (59) Bostick, B. C.; Fendorf, S.; Helz, G. R. Differential adsorption of molybdate and tetrathiomolybdate on pyrite (FeS₂). *Environ. Sci. Technol.* **2002**, *37*, 285–291.
- (60) Saiki, Y.; Fukuzaki, M.; Sekine, T.; Kino, Y.; Kudo, H. Technetium(VII) sulfide colloid growing observed by laser-induced photoacoustic spectroscopy. *J. Radioanal. Nucl. Chem.* **2003**, *255*, 101–104.
- (61) Weber, F.-A.; Voegelin, A.; Kaegi, R.; Kretzschmar, R. Contaminant mobilization by metallic copper and metal sulphide colloids in flooded soil. *Nat. Geosci.* **2009**, *2*, 267–271.
- (62) Yin, Y.; Rioux, R. M.; Erdonmez, C. K.; Hughes, S.; Somorjai, G. A.; Alivisatos, A. P. Formation of hollow nanocrystals through the nanoscale Kirkendall effect. *Science* **2004**, *304*, 711–714.
- (63) Almahamid, I.; Bryan, J. C.; Bucher, J. J.; Burrell, A. K.; Edelstein, N. M.; Hudson, E. A.; Kaltsoyannis, N.; Lukens, W. W.; Nitsche, H. Electronic and structural investigations of technetium compounds by X-ray absorption spectroscopy. *Inorg. Chem.* **1995**, *34*, 193–198.
- (64) Terry, J.; Grzenia, B.; Papagiannopoulos, D.; Kyger, J.; Jurisson, S.; Robertson, J. D. Structural determination of Tc radiopharmaceuticals and compounds using X-ray absorption spectroscopy. *J. Radioanal. Nucl. Chem.* **2005**, *263*, 531–537.
- (65) Darab, J. G.; Amonette, A. B.; Burke, D. S. D.; Orr, R. D.; Ponder, S. M.; Schrick, B.; Mallouk, T. E.; Lukens, W. W.; Caulder, D. L.; Shuh, D. K. Removal of pertechnetate from simulated nuclear waste streams using supported zerovalent iron. *Chem. Mater.* **2007**, *19*, 5703–5713.
- (66) Lamfers, H. J.; Meetsma, A.; Wiegers, G. A.; De Boer, J. L. The crystal structure of some rhenium and technetium dichalcogenides. *J. Alloys Compd.* **1996**, *241*, 34–39.
- (67) Johnson, R. L.; Nurmi, J. T.; O'Brien Johnson, G.; Fan, D.; O'Brien Johnson, R.; Shi, Z.; Salter-Blanc Alexandra, J.; Tratnyek, P. G.; Lowry, G. V. Field-scale transport and transformation of carboxymethylcellulose-stabilized nano zero-valent iron. *Environ. Sci. Technol.* **2013**, *47*, 1573–1580.
- (68) Liu, Y.; Terry, J.; Jurisson, S. S. Potential interferences on the pertechnetate-sulfide immobilization reaction. *Radiochim. Acta* **2009**, *97*, 33–41.